31 March 2023

Deliverable 4.3
Impact in the European Research Area

Contractual Date:	30-09-2022
Actual Date:	31-03-2023
Grant Agreement No.:	951886
Work Package:	WP4
Task Item:	Task 4.2
Nature of Milestone:	R (Report)
Dissemination Level:	PU (Public)
Lead Partner:	INRIM
Document ID:	CLONETS-M30-003
Authors:	D. Calonico (INRIM), P. Tuckey (OBSPM)

The research leading to these results has received funding from the European Union's Horizon 2020 research and innovation programme under Grant Agreement No. 951886 (CLONETS-DS).

Abstract
This document highlights impacts of the proposed CLONETS Research Infrastructure in the European Research Area.

Table of Contents

Table of Figures

1 Executive Summary/Introduction

This document follows on from the Science Case, reference [43], and the Technical Design Report, reference [1], of the CLONETS-DS project. Its purpose is to illustrate and facilitate the impact of the pan-European fibre infrastructure for time and frequency dissemination proposed by CLONETS-DS on research in the European Research Area, by providing details of how the infrastructure will be used for key applications. It also summarises the fibre infrastructures for time and frequency dissemination which are currently being operated by the CLONETS-DS partners, and the possibilities for using them for proof-of-concept demonstrations.

2 Application of the infrastructure to impact areas

This chapter discusses practical aspects of the use of the proposed infrastructure in key application areas. The research infrastructure is referred to throughout by the term European Core Network (ECN), following the terminology of the Technical Design Report [1].

2.1 Existing infrastructures and test-bed capabilities for proof-of-concept demonstrations

The following table lists the fibre infrastructures for time and frequency currently being operated by CLONETS-DS partners, and provides brief information on the possibilities for proof-of-concept demonstrations for research applications. More detailed information is available through the given points of contact.

Country and name of the infrastructure or test bed	Description of the kinds of possible tests	Access conditions and points of contact
Austria, Austrian Academic Computer Network – ACOnet	Link stability tests (Innsbruck-Vienna) Comparison of local optical oscillators (probably in network topology) Maser comparison via optical links	Conditions depend on the type of activity. Christian Panigl, Vienna University Computer Center, Department ACOnet & VIX, Universitaetsstrasse 7, 1010 Vienna Thorsten Schumm, Atominstitut, TU Wien, Stadionallee 2, 1020 Vienna
Czech Republic, CITAF (Czech Infrastructure for Time and Frequency)	Coherent frequency on different wavelengths, modulated RF time and frequency. Many options.	Depends on test type and requested duration. josef.vojtech@cesnet.cz or vladimir.smotlacha@cesnet.cz
France, REFIMEVE national infrastructure	REFIMEVE is an operational network and thus cannot be used as a photonic testbed. By contrast, REFIMEVE can welcome EU researchers to demonstrate user cases.	Request to REFIMEVE governing board. In any case, there is a user charter to be signed before access to the REFIMEVE network. anne.amy-klein@univ-paris13.fr

Country and name of the infrastructure or test bed	Description of the kinds of possible tests	Access conditions and points of contact
	Data generated by REFIMEVE are available upon reasonable request (OPEN science), including characterisation of the frequency transfer. Tests for interconnection with REFIMEVE can be made in Paris and Geneva.	
Germany, several point-to-point connections	PTB-LUH: testbed for quantum communication PTB-MPQ: testbed for time & frequency, geodesy, VLBI PTB-Strasbourg: international testbed for optical clocks, general time & frequency issues	Financial support of fibre lease, cooperation contract. jochen.kronjaeger@ptb.de
Italy, Italian Quantum Backbone (and cross-border link to Modane, France)	Fundamental physics, metrology; quantum communication; timing for industry	Access conditions by agreement. c.clivati@inrim.it
Poland, national infrastructure for time and frequency distribution	Project PionierLab: national infrastructure for time and RF frequency distribution. Project NLPQT: national infrastructure for distribution Optical Frequency from Polish optical clocks. Both networks are available for scientific research and as a testbed for optical clocks, general time & frequency issues	wojbor@man.poznan.pl
Spain, RedIRIS network	Optical carrier frequency dissemination is expected in the future.	A direct or indirect connection to RedIRIS is required. Héctor Esteban Pinillos Real Instituto y Observatorio de la Armada hesteban@roa.es

Country and name of the infrastructure or test bed	Description of the kinds of possible tests	Access conditions and points of contact
Switzerland, Swiss Stabilized Optical Fibre Network	Connect existing networks of different wavelengths (e.g. CH44 to CH07)	By agreement. SWITCH: fabian.mauchle@switch.ch Federal Institute of Metrology METAS: jacques.morel@metas.ch
United Kingdom and France, London-Paris link	Not available as a test bed	rachel.godun@npl.co.uk

2.2 Data format for frequency measurements

The data and procedures for measurements using the ECN are described in detail in the Technical Design Report [1]. In this section we consider the application to frequency measurements made by ECN users.

A user of ECN frequency services has an ECN terminal equipment which provides access to a reference frequency, ν_{int}. The user uses this reference as the basis for their frequency measurements, for example the user may measure frequency offsets $\nu - \nu_{int}$, or ratios ν/ν_{int}, with respect to the reference.

The reference frequency is monitored and characterised by the ECN, as delivered at the user's terminal. The characterisation consists of a time series of successive data triples, of format:

$$(t, \nu_{int}(t), Q(t))$$

where:

- t is a timestamp, expressed as a Modified Julian Date (MJD). Successive values are normally separated by 1 s intervals;
- $\nu_{int}(t)$ is the value of the reference frequency (1 Hz bandwidth) at time t (normally represented as the offset from the nominal value);
- $Q(t)$ is the quality indicator of the provided reference frequency at time t, a Boolean value indicating correct functioning of the CLONETS signal distribution to the user at the stated time. The series of values $Q(t)$ constitutes a mask allowing the user to exclude measurements made at times when the reference frequency provided by the ECN is unusable due to network or other incidents.

The characterisation of the reference frequency delivered to the user by the ECN is completed by an estimate of its systematic uncertainty. This quantity is constant over long time intervals, aside from signal distribution incidents accounted for by the quality indicator, and is verified and updated

periodically by calibration campaigns. Its value is typically smaller than the statistical fluctuations of the reference frequency, see for example chapter 5 of Tennis' thesis [40] and references therein.

The reference frequency characterisation provided by the ECN is sufficient to allow the user to perform frequency measurements ν of moderate total uncertainty, of the order of 10^{-14} (relative).

To achieve smaller uncertainties, users must use the method of synchronised frequency comparisons, described in [1] and illustrated by *Figure 1* (reproduced from that reference). In this method, each user records pairs of data consisting of a timestamp, t' and t'' in *Figure 1*, and a frequency measurement relative to the ECN frequency, $\nu_{int}(t') - \nu_1(t')$ and $\nu_{int}(t'') - \nu_2(t'')$. (Each user must take into account the mask provided by the quality indicator for their own access to ν_{int}.) Provided the measurements of the two users are sufficiently well synchronised, for example at the ms level (see [1]), they can be combined to eliminate the ECN reference frequency to obtain a relative frequency measurement between the two users, $\nu_2(t'') - \nu_1(t')$, which has an extremely low contribution from the ECN to its total uncertainty. This is the relative frequency service defined in [1].

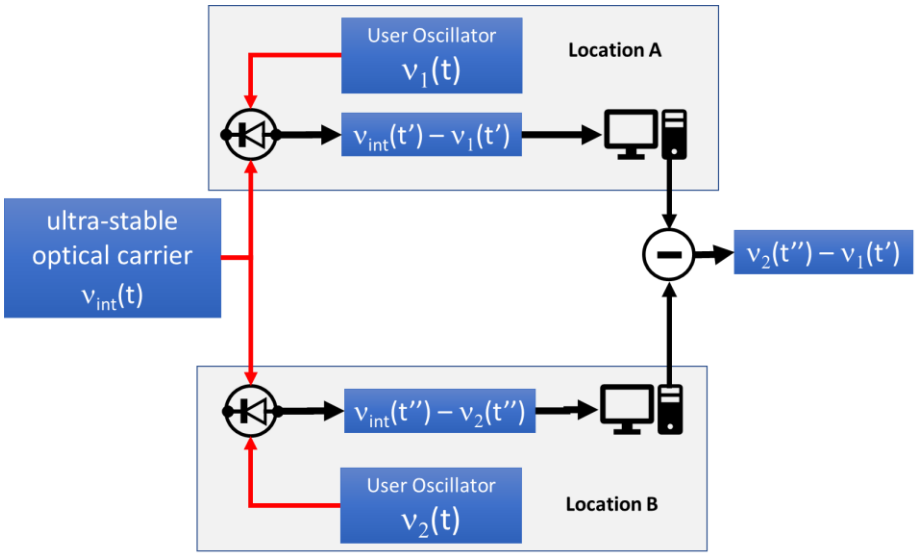

Figure 1: Basic relative frequency service for optical signals provided by the network

If in addition one of the user oscillator frequencies, for example $\nu_2(t'')$, has a very small uncertainty, such as in the case of a National Metrology Institute, then the other user can combine its value with the result of the relative frequency measurement, to obtain the value of their own frequency, $\nu_1(t')$, with an extremely low uncertainty contribution from all parts of the measurement external to their own site, up to and including their ECN user terminal. This is the absolute frequency service defined in [1].

2.3 Data format for VLBI geodesy experiments

The data format for VLBI Geodesy experiment should consist of a first meta-data table like the following example:

Location of Time reference (UTC(k) lab)	
Location of geodetic user	
Description of fiber link	
Equipment at UTC(k) lab	
Equipment at geodetic user	
Scheduled time for campaign	

Then, for the data themselves, the preferrable format is:

(MJD; frequency difference)

where the "MJD" is a time stamp expressed in Modified Julian Date, with 8 significant digits (to cover the seconds in a day); "frequency difference" is the frequency difference between the local hydrogen maser used as reference at the VLBI station, and the frequency disseminated by the optical link. Of course, an optical frequency comb is used at the VLBI station to convert the optical frequency to the radio frequency of the maser (100 MHz preferred).

2.4 Guidelines for frequency dissemination for non-NMI users

In this section we will describe how frequency dissemination can be implemented for non-NMI users in fields such as geodesy and high-resolution spectroscopy.

Very Long Baseline Interferometry

The primary VLBI observables for high-precision astrometry are: the interferometric phase ϕ, the phase difference between the signals received at a pair of antennas or equivalently the phase delay (the phase in radians divided by the frequency in Hz, in seconds; $\tau_\phi=1/2\pi\ \phi/\nu$) the frequency derivative or group delay (the rate of change of phase with frequency, in seconds $\tau_g=1/2\pi\ \delta\phi/\delta\nu$) and the phase time derivative (usually as delay rate in seconds/second; $1/2\pi\nu\ \delta\phi/\delta t$).
Following the standard nomenclature (Thompson et al. 2017) the residual phase values or errors after subtracting the a-priori model contributions from the measured values at the time of the correlation or post-processing for observations of a target source (A) for a given baseline as a function of time and frequency are shown as a sum of contributions:

$$\phi_A(t,\nu)=\phi_{(A,pos)}+\phi_{(A,str)}+\phi_{(A,geo)}+\phi_{(A,tro)}+\phi_{(A,ion)}+\phi_{(A,instr)}+\phi_{(A,thermal)}+2\pi n$$

where the $\phi_{(A,pos)}$ (the most relevant in astrometry) arises from inadequacies in the a-priori knowledge of the source position. $\phi_{(A,str)}$ stands for the contribution from the structure in extended sources. $\phi_{(A,geo)}$ arises from the model uncertainties in the geometry of the array including the orientation of the Earth among others; $\phi_{(A,tro)}$ and $\phi_{(A,ion)}$ arise from mis-modelling of propagation medium effects as the sky signal transverses the Earth due to refractivity variations in the troposphere and ionosphere along the line of sight, respectively. $\phi_{(A,instr)}$ refers to the instrumental instabilities (including the clock term). The purpose of astrometric calibration is the identification and elimination of these extrinsic terms. $\phi_{(A,thermal)}$ stands for the thermal noise term and is related to the sensitivity of the instrument, thus setting the ultimate potential astrometric limit, with a standard deviation by $\sigma(\phi_{(A,thermal)})\sim 1/SNR$ in radians, where SNR is the signal-to-noise ratio of the fringe detection. Finally, $2\pi n$ stands for an unknown integer number n of phase cycles that represents the inherent ambiguous nature of the measured phases; n can vary between observations of the same source at different times, and between different sources. It sets the greatest challenge for astrometry using the phase observable.

The group delay observable is determined from the phase slope over the discrete frequencies in the spanned observed bandwidth. A similar description as in the Equation above applies to the group delay residuals but without the the 2π ambiguity term which makes it more usable for absolute positional measurements. The group-delay is the observable used for VLBI geodesy and absolute astrometry.

At cm wavelengths, as in geodetic VLBI, also in radio astrometry and imaging of radio sources with sub-milliarcsecond resolution the main contaminant of interferometric phase stability is caused by tropospheric fluctuations. Radio Astrometry is the branch of radioastronomy that aims at determining radio source absolute positions with the minimum possible uncertainty (for a recent review see Rioja & Dodson [2]). The clock frequency reference instability affects phase measurements in baseline antenna pairs but appears to be subdominant with respect to troposphere and ionosphere effects in all cm wavelength observations. Rioja and Dodson [3] studied the combined effects of clock frequency reference instability and tropospheric instabilities.

In a series of mm-VLBI simulations at the frequencies of 86, 175 and 350 GHz. A simple phase self-calibration scheme was compared with a more advanced method (Frequency Phase Transfer (FPT) calibration, Rioja & Dodson,[4]. They also used two clock types (classical H-masers and more stable Cryo-cooled Sapphire Oscillators, CSOs). The tropospheric fluctuations were modelled for a choice of four weather conditions, i.e. Very Good (V), Good (G), Typical (T) and Poor (P), adjusting the modified coefficient of the spatial structure function of the troposphere to values 0.5, 1, 2 and $4 \times 10{-}7m{-}1/3$, respectively, with the assumption of Kolmogorov turbulence.

They used an updated version of the simulation software ARIS to generate synthetic datasets which replicate the interferometric visibilities obtained from a correlator for a given observing configuration, i.e. coordinates of the telescopes and celestial target, observing frequencies, bandwidth, atmospheric conditions and noise contributions from station frequency standards for both H-masers and CSOs. The calibrated complex visibilities were Fourier transformed and deconvolved using standard imaging procedures with the AIPS task IMAGR, in order to produce a synthetic image. The Fractional Flux

Recovery (FFR) quantity, defined as the ratio between the peak flux in the map divided by the source model flux, was extracted and used as the figure of merit to evaluate and compare the coherence losses for each combination of clock, troposphere stability and phase calibration scheme. Larger values of FFR correspond to smaller coherence losses, which in turn lead to higher sensitivity (i.e. SNR) in the synthetic map.

The results were shown in steps: in case 1 only clock instability is present. In case 2 only atmospheric instability is present, in case 3 clock and atmosphere noise are merged, in case 4 dual frequency observations are simulated in order to implement the FPT phase mitigation scheme.

Their simulations show that in most situations the tropospheric fluctuations constitute the dominant contribution to the coherent losses at mm and sub-mm wavelength observations, their impact increasing with the observing frequency and/or worsening weather conditions, which in turn limit the coherence time (timespan after which the visibilities significantly decorrelate) and source sensitivity (and hence SNR). Substituting an H-maser clock with a CSO high-performing clock at the observing stations (case 1) brings a dramatic improvement in FFR with negligible coherence losses (<0.5% in 6-min integration time) even in the worst condition (higher frequency: 350 GHz) with respect to H-maser performance of 35% coherence loss. Comparing atmosphere and clock (case 2) one notices that H-maser and troposphere instabilities attain comparable coherence losses (~10% in 2-min integration time) at 350 GHz when troposphere is in Good weather conditions. In all other cases the atmosphere dominates over clock except for Very good weather conditions, which are met only by extremely good mm observing sites such Chajnator Observatory (ALMA site). The Phase Mitigation provided by the FPT calibration scheme and the auxiliary usage of Water Vapour Radiometers allow for the notable sensitivity improvement even at 175 GHz: the increased sensitivity obtained from the CSO with respect to the H-maser in observations at 175 GHz with best (V) weather conditions are estimated to be 9% and 13%, for coherence losses of 20% and 10%, respectively. At 350 GHz, the estimated increased sensitivity values are 22% and 41%, respectively, in V weather conditions. For G weather these are 11% and 18%. Maximum values of increased sensitivities are estimated for the case of WVR-corrected atmospheres (W) at 350 GHz, equal to 60% and 120%, for coherence losses of 20% and 10%, respectively. In all cases, the estimated values for increased sensitivities are larger for lower acceptable coherence losses.

A case study for high-frequency usage of frequency reference distributed by optical fibre links is the Korean VLBI Network (KVN,[5]) an array of three 25-m antennas separated by a few hundred km currently operating a Compact Triple-band Receiver up to 129 GHz (CTR, [6]). Rioja and Dodson successfully applied updated versions of their phase mitigation scheme on KVN [7] and in a few years an upgrade at 230 GHz is foreseen. This could be a good opportunity to test a common-clock topology disseminating a highly stable frequency standard (ultimately provided by an optical clock) to the three KVN antennas via a coherent wave optical fibre network. In this particular case, where the clock related frequency instability can emerge over the tropospheric effects, VLBI astrometry and radio imaging would benefit from this advanced set-up.

Geodetic VLBI

The future of geodetic Very Long Baseline Interferometry (VLBI), a space geodesy technique [8], using the group delay of radio wave fronts coming from a catalog of extragalactic radio sources and received by pairs of radio antennas in an array to study tectonic plate motion, pole wobbling and variations in the length of day (Earth Orientation Parameters, EOPs) was set by the design of the VLBI Global

Observing System (VGOS, [9]). VGOS will comprise a network of up to 28 stations (9 are completed and working, 10 are under commissioning and other 9 are planned) with antenna dish diameters of 12-13m, a large slewing speed (more than 6 deg/s), a System Equivalent Flux Density of about 2500 Jy, a frequency range of 2-14 GHz in 4 sub-bands, and a recording rate of up to 32 Gbps. When all these specifications are met it will be possible to achieve a 4-ps weighted RMS on the group delays of the radio wave fronts reaching pairs of antennas (baselines) in 24-h long sessions in continuous operation. This is the demanding goal in order to obtain a 1-mm position uncertainty and 0.1-mm/yr velocity uncertainty on the observing station mark points and an accuracy on the polar motion of 50 micro-arcsec and 3-5 micro-seconds on the determination of UT1-UTC. The main contribution to the uncertainty in the group delay modelling is caused by tropospheric delay.

To better understand the impact of random errors on geodetic products, Monte Carlo simulations were performed by Petrachenko et al. [10] that used realistic models for the troposphere delay variations, hydrogen maser frequency stability, and Gaussian-noise-like delay errors. Various strategies were tested to determine which were most effective for minimizing the impact of random errors on the geodetic products. By far the most effective strategy was to significantly increase the number of angularly well-distributed observations per unit time, with one observation every 30 s achieving the 1-mm performance target in the simulation results, largely attributable to enhanced atmospheric sampling.

In Niell et al. [11] a more in-depth evaluation of the required clock frequency stability is provided: at short times, up to the scan length, which can be up to 30 s, the stability must be sufficient to produce no significant loss of coherence at the highest observing frequency. This corresponds to an Allan deviation of about 1 x 10-14 at 30 s. At longer time scales the clock stability must be good enough that temporal variations in the time-base generated by the reference frequency do not add significant noise to the group delays. To keep such noise below a few times the median per-scan delay uncertainty of ~ 4 ps, the stability should be better than ~ 1 x 10-14 at 1200 s of integration time. Petrachenko et al. [10] indicated that a combined stability of 10-14 at 50 minutes for the two stations forming a VLBI baseline is sufficient for the frequency reference to not be a limiting error source.
Regarding the timing requirement (station clock synchronisation), a pair of stations forming a baseline can obtain visibility fringes at correlation stage easily, even if the timing uncertainty is a few tens of ns. After the implementation of software correlation (DiFX, [12]) and the continuing increase in computing power at correlator centres, a timing accuracy reachable with optical fibre dissemination techniques is not strictly necessary to set up the iterative correlation scheme.

More interesting is the reverse argument: the possibility of using the VGOS network of antennas in synergy with optical fibre links connecting National Metrological Institutes (NMIs) and VGOS stations to compare high performing (optical) atomic clocks at intercontinental distances.

A study pointing in this direction is described in [14] with results detailed in [15] in which a baseline was formed between two small broadband antennas (2.4-m diameter Marble antennas mounting custom-made broadband Ninja feeds) were used in a node-hub scheme to transfer the frequency reference between two optical lattice clocks located in Italy and Japan. A similar experiment, using the VGOS antennas of Ishioka (Japan) and Onsala (Sweden) could be attempted. In this particular case, two coherent wave optical fibre links should be set up: one between Onsala Space Observatory and RISE institute optical clock lab and another one between the Ishioka VGOS station and the NICT optical clock lab. The planned deployment of a VGOS antenna in the ASI Centre for Space Geodesy in Matera

(Italy) would also allow to make use of the Italian Quantum Backbone coherent wave optical fibre link connecting INRiM and ASI-CSG Matera station [15], thus opening the INRiM Yitterbium optical lattice clock to the VGOS network.

Relativistic geodesy

The possibility of using optical clocks to measure the relativistic frequency shift caused by the Earth gravitational potential and thus measure absolute height differences (for a review see [16]) is a new addition to geodetic methods. Einstein's general relativity theory predicts that an ideal clock at rest will run at a slower rate, when under the influence of a gravitational potential compared to a clock outside of it. For two clocks placed at different sites with local gravitational potentials V_1 and V_2 this relativistic frequency shift is expressed in terms of the difference in clock ticking rate, i.e. the difference of clock frequencies f_1 and f_2 according to:

$$\Delta f/f=(f_1-f_2)/f=-\Delta V/c^2 \qquad \text{where } \Delta V=V_1-V_2$$

The idea of using clocks to determine potential (and corresponding height) differences in geodesy dates back to Bjerhammar and Vermeer [17][18][19]. This 'chronometric levelling' offers the great advantage of being independent of any other geodetic data and infrastructure, with the perspective to overcome some of the limitations inherent in the classical geodetic approaches. [18] also gave the following remarkable definition for the geoid, stating that 'The relativistic geoid is the surface where precise clocks run with the same speed and the surface is nearest to Mean Sea Level'. In this contest, the (classical) definition of the geoid as an equipotential surface is, to the level of approximation used above (roughly a few parts in 1019), identical with a surface on which clocks tick with the same rate. The frequency difference between two clocks, observed via an appropriate link, directly gives a gravity potential difference between the two sites. Optical clocks are approaching the 10-18 regime (or below) in fractional frequency uncertainty that corresponds to a height uncertainty of 1 cm (or better). This would be an absolute height measurement, independent from geometric levelling determination [20] which is at the moment affected by uncertainties of a few tens cm on long distance (on hundreds of km).

With the advent of space-based methods that allow global measurements to be made (with Global Navigation Satellite System 24 hours a day, seven days a week), it became possible to define a purely geometrical global coordinate system with position accuracies at the level of one centimetre (or below), allowing the detection of plate tectonic and other deformations. These coordinate systems are primarily Cartesian and have their origin at the centre of mass of the Earth, with the axes aligned in a well-defined manner to the outer surface of the Earth. The Cartesian coordinates can also be transformed into equivalent ellipsoidal coordinates based on a given reference ellipsoid with ellipsoidal latitude, longitude, and height, all being again purely geometrical quantities. However, historically, before the era of GNSS, coordinate systems in geodesy were divided into (geometry-based) horizontal coordinates (latitude and longitude) and a (potential-based or physical) vertical coordinate called height, which was a consequence of the methods available for making measurements. These physical heights are based on equipotential surfaces within the Earth's gravity field, along which fluid will not flow. Consequently, equipotential or level surfaces are of paramount importance for geodesy, oceanography, geophysics, and other disciplines to define (physical) heights on the continents and for the dynamic ocean surface in order to answer questions on the direction of fluid (water) flow.

National geodetic height systems based on classical terrestrial geometric levelling and satellite-based GNSS measurements exhibit discrepancies at the decimetre level [21]. Optical clocks thus offer an attractive way to resolve these discrepancies, as they combine the advantage of high spectral resolution with small error accumulation over long distances.
Combining the use of portable optical clocks with high-performance frequency dissemination techniques allows to perform chronometric levelling-based height measurements also in areas away from National Metrological Institutes but along the routes of optical fibre networks. A round-trip phase noise cancellation scheme in the coherent wave optical fibre link allows a frequency stability of ~ 10-19 making the optical clock frequency transfer uncertainty caused by the fibre link almost negligible. This would allow a very fast height measurement response making possible the assessment of geodynamic effects on time scales of a few hours [22]. An example could be mass shifts in the upper layer of the Earth's crust due to groundwater changes but not accompanied by any position change of the instrument site (no surface deformation, no distance change with respect to the geocenter).

Satellite Laser Ranging

Satellite Laser Ranging (SLR) fundamentally relies on the (rate) x (time) = distance relationship to ultimately estimate tracking sites positions which can then be used to monitor the changes in a variety of Earth processes (e.g. tectonic motions, polar motion, Earth rotation, tidal and gravitational forces). The raw SLR "range" is a time interval measurement. The actual range is defined as one half of the product of the speed of light and the elapsed time between the emission of a laser pulse and its reception at the same tracking site (the SLR station) after having been reflected off a satellite equipped with retro-reflecting mirrors (e.g. LAGEOS). When a large number of these temporally and geographically distributed range measurements are ordered by time and location each range can be considered to represent a constraint in the solution of the numerically integrated equations of motion describing satellite orbit. The adjustments between the a-priori predicted and observed ranges are used to form the linear least square equations which best satisfy all of the range information simultaneously. The resulting system of equations is then solved to yield the time-averaged three dimensional coordinates of the tracking stations. The rate at which the station positions with adequate tracking histories change as a function of time is considered to reflect tectonic plate motions, Earth Orientation Parameters (EOPs) and local deformations.

SLR is currently using up to 43 station world-wide [23] and contributes to the determination of the International Terrestrial Reference Frame (ITRF, [24]). The SLR data products and station coordination is provided by the International Laser Ranging Service (ILRS, a service of the International Association of Geodesy). The International Earth Rotation and Reference Systems Service (IERS) set the goal for the Global Geodetic Observing System (VLBI, GNSS, SLR and DORIS) to 1 mm position uncertainty and 0.1 mm/yr velocity uncertainty for the reference points of the tracking stations. SLR, being a two-way space-ground optical ranging system based on relatively slow moving (< 10 km/s) targets (retro-reflecting mirror cubes mounted on earth orbiting satellites), can achieve IERS specifications with an accuracy in the firing laser timing of a few tens of ns (the International Laser Ranging Service (ILRS) recommendations of $\delta t < 100$ ns [25]. The sub-picosecond timing accuracies achievable by time reference dissemination on optical fibre links project could instead be beneficial to the optical laser time transfer techniques, in particular in synchronising ground stations in ground-space-ground two-way experiments [26][27]. Recent experiments of time transfer by laser ranging around the Earth, such as Laser Time Transfer [28], T2L2 (Jason-2, [29]), and ELT (ISS, [30]) between 36,000 and 500 km, proved the possibility to establish time links into space or ground links via a space equipment with an unprecedented stability (one to a few ps over thousands of seconds of integration time) and accuracy (100 ps currently and 25 ps expected at GOW, Germany with ELT/ACES), even on a operational basis.

To achieve this performance, the primary stations behind these experiments have been playing an important role in maintaining a high stability of the 1 PPS distribution signals on the long term and in accurately calibrating most of their T/F equipment. Compensated optical fibre links can also contribute to the control of systematic errors in optical time transfer by SLR (see [31] for the work done at Wettzell Observatory). Closure measurements can also be used to identify and remove systematic errors in SLR measurements.

Implementation Guideline: the demonstration in Italy of a long-haul frequency transfer for Geodetic VLBI.

In this Section, we describe the implementation in Italy of a distribution for non-NMI, specifically VLBI users, that can be used as a guideline.

We disseminate an optical frequency reference from a Metrology Institute to two distant radio telescopes, separated by a baseline of 600 km in Italy, using a 1739-km-long phase-stabilized fiber link. A microwave signal is synthesized at each telescope site using an optical frequency comb and feeds the VLBI synthesis chain. The described infrastructure allows the dissemination of microwave and optical frequency standards to multiple sites, with up to 2 orders of magnitude improvement in accuracy and stability as compared to local hydrogen masers or fiber-based RF dissemination. As a proof-of-concept experiment, we used this infrastructure in a 24 h geodetic VLBI campaign where the two Italian telescopes shared a common fiber-delivered clock signal. These experiments demonstrated the feasibility of this approach and open up the possibility of more advanced studies on VLBI limiting effects.

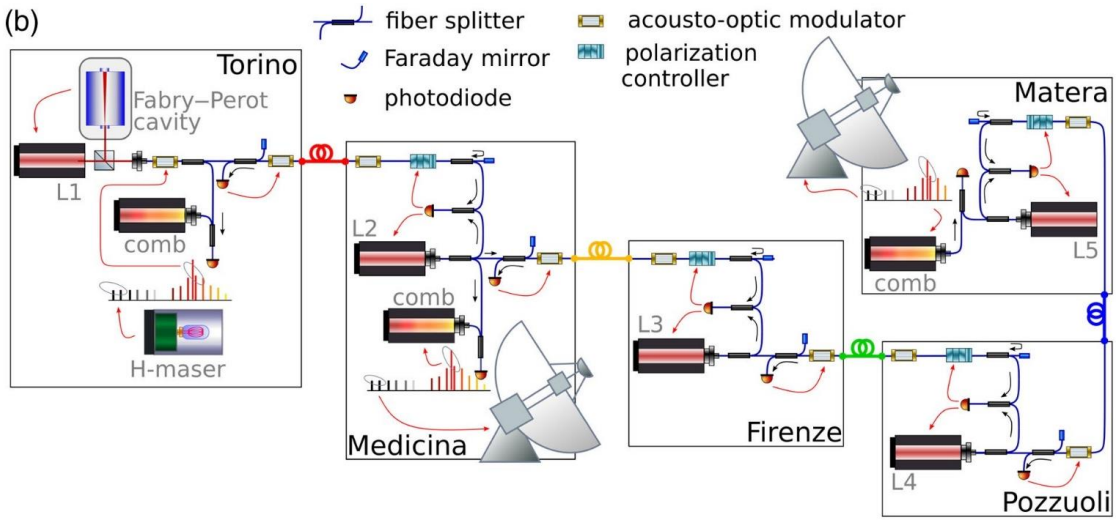

Figure 2: (a) A map of the fiber-based network for VLBI in Italy. Different colors indicate the four segments of the link. Red, Torino-Medicina, 535 km. Yellow, Medicina-Firenze, 149 km. Green, Firenze-Pozzuoli, 668 km. Blue, Pozzuoli-Matera, 387 km. Purple, connection to the French border and European atomic clock network. Circles, optical amplification sites. (b) A block diagram of the infrastructure. L1, master laser, frequency stabilized on a high-finesse Fabry–Perot cavity and on a H-maser-referenced optical comb. L2–L5, local regenerating lasers, phase-stabilized to the link-delivered optical signal. At the Medicina and Matera VLBI sites, the optical signal is coherently divided to the RF domain using local optical combs. Phase noise of the connecting fibers is detected by comparing the round-trip radiation to the local light in a Michelson interferometric scheme, and corrected using acousto-optic modulators. Red arrows indicate referencing and active feedback systems; black arrows indicate the direction of light.

Our infrastructure is based on the dissemination of a common frequency reference from the Italian Metrology Institute (INRIM) located in Torino, to two radio telescope sites located in Medicina and Matera, operated, respectively, by the National Institute for Astrophysics and the Italian Space Agency. A map of the infrastructure in its present status is shown in Fig. 6.20(a). It builds upon the connection between INRIM and Medicina Radio Observatory, which has been operative since 2015 [31], and extends the baseline to the Matera Space Geodesy Centre. The link also connects major research facilities of the Country, namely the European Laboratory for Non-Linear Spectroscopy (LENS) in Firenze [32][33] and the National Institute for Optics, which is part of the National Research Council (CNR-INO) in Pozzuoli, and is part of the atomic clock network under development in Europe [9]. Figure 6.20(b) shows a block diagram of the overall dissemination chain. It is based on the transmission of a laser signal at 1542.14 nm, whose frequency is stabilized on a high-finesse Fabry–Perot cavity to achieve a linewidth of a few Hz. On the long term, the laser's frequency is referenced to a hydrogen maser traceable to the definition of the second in the International System of units (SI) using an optical comb. Referencing to the INRIM Yb optical lattice clock [34] is also possible. The ultrastable laser is sent to the remote laboratories using fibers of the telecom network, to which operators have access for maintenance and upgrade. The backbone is divided in four cascaded segments, each identified by a different color in Fig. 6.20: Torino-Medicina, 535 km (red); Medicina-Firenze, 149 km (yellow); Firenze-Pozzuoli, 668 km (green); Pozzuoli-Matera, 387 km (blue). At each terminal, a diode laser is phase-locked to the incoming light and is injected into the next segment. Light is also partly reflected back toward the previous terminal and here compared to the launched radiation. This allows detection and cancellation of the noise added to the optical phase during the round trip into the connecting fiber [35]. Similarly, return light from the following terminal is compared to local light and used to stabilize the fiber in between. At the Medicina and Matera terminals, the local laser that is phase-locked to the incoming light is coherently divided down to 100 MHz using an optical frequency comb. The synthesized RF signal is therefore phase-coherent with the original signal located in the transmitting laboratory.

The link segmentation is beneficial from several points of view [36]. First, phase-stabilization of fiber segments shorter than the full link allows a larger control bandwidth, as this latter is limited to $c/4L$, with L being the span length and c the speed of light into the fiber [35]. In our setup, the fiber noise was stabilized on bandwidths of 60 Hz, 150 Hz, 70 Hz, and 100 Hz on the four spans, respectively, while the locking bandwidth would be limited to <30 Hz if the full length of the link was stabilized. In addition, optical regeneration allows a better managing of the optical loss, which would exceed 480 dB for the full link and could not be recovered with erbium-doped fiber amplifiers (EDFAs) only. At the same time, it filters broadband optical noise introduced by EDFAs. Finally, at every node, an ultrastable, optical reference traceable to the SI unit is available, which can be used for local applications. This approach is particularly effective in our facility, where the same reference signal has to be provided to multiple sites.

VLBI experiments have a typical duration of several hours or days; hence, continuous operation and phase coherence of the disseminated reference must be maintained over these time scales. The most critical aspect to meet these requirements is the robustnessofthevariousopticalphase-lockedloopsinvolvedinthechain, which in turn depends on the optical beatnotes' signal-to-noise ratio at detection. This is mainly affected by variations in the signal polarization as it travels the link, and gain instability of the EDFAs, which can lead to >10 dB variation in the beatnotes' power. To cope with such issues, polarization and gain of the EDFA chain are actively stabilized, allowing up to several days of continuous uptime. Residual failures are due to fast flips of the signal polarization, which we attributed to human work along the line and cannot be tracked by our system. To further improve the uptime and reduce the operator intervention, we are investigating novel phase detection techniques based on dual-polarization receivers [37], and we are upgrading the system to allow completely unmanned failure-recovery capability. With these solutions, optical frequency dissemination can move to a regime where the maintenance activity becomes similar to that required for local standards [36].

Figure 6.21(a) shows the phase noise introduced by the four link segments. All of them show similar features: noise is dominated by a flicker-phase process in the low-frequency range, with a peak around 12 Hz that is attributed.

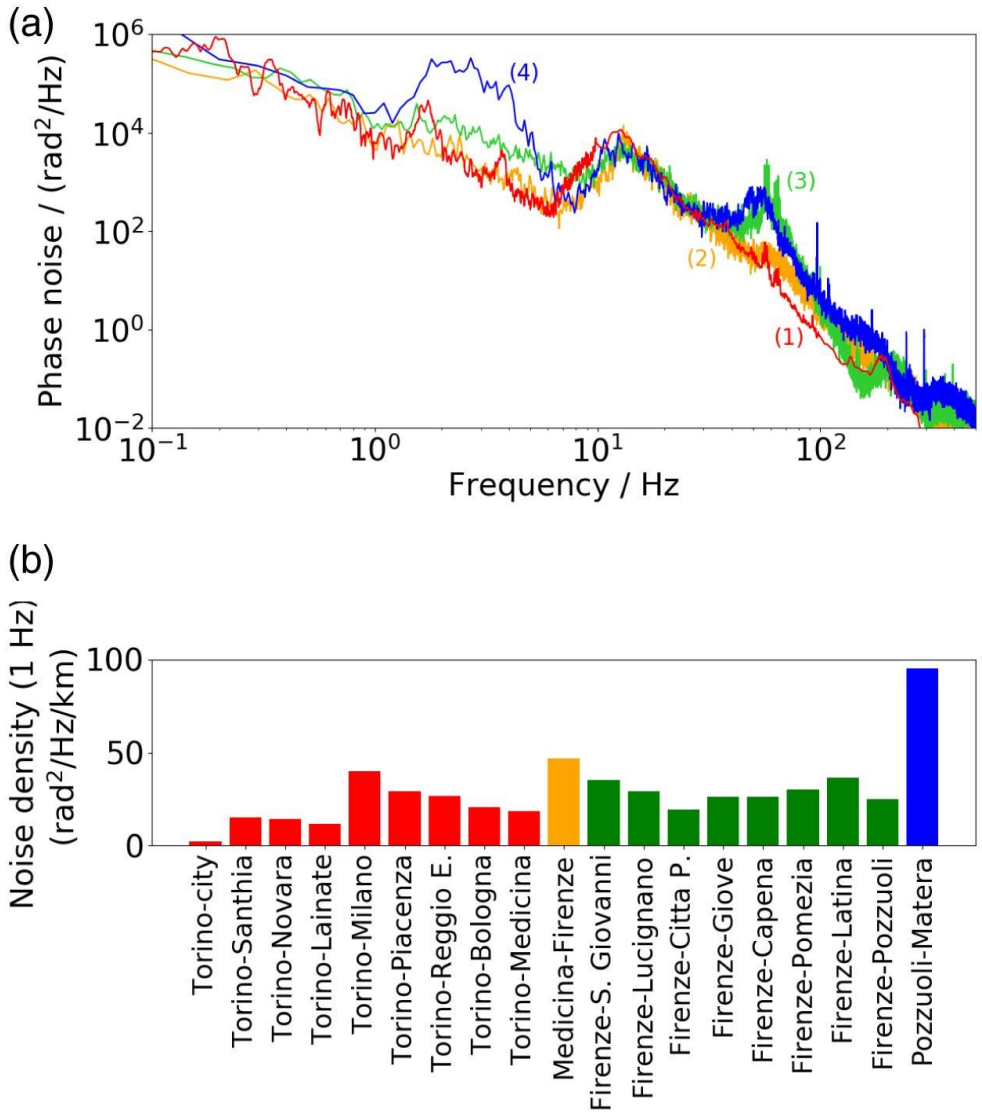

Figure 3: (a) Phase noise of the four link segments. (1) Red, TorinoMedicina; (2) yellow, Medicina-Firenze; (3) green, Firenze-Pozzuoli; (4) blue, Pozzuoli-Matera. (b) Spatial noise density at 1 Hz Fourier frequency for various spans of increasing length. Different colors indicate different segments.

to human activities such as traffic and building vibrations. The segment connecting Pozzuoli to Matera (blue) shows a significant noise excess around a few Hz Fourier frequency. This is attributed to the presence of about 5 km of aerial cables, which are presumably subject to dangling due to wind. This span also shows higher polarization instability. During the EDFA installation, we were able to measure the integrated fiber noise between the transmitting terminal and various intermediate locations. These measurements were made by reflecting back the light at the intermediate stations and recording the fiber noise in an unstabilized condition. Figure 6.21(b) shows the phase noise power spectral density at 1 Hz Fourier frequency for various fiber spans, normalized to the span length. This gives indication of the average spatial density of the noise as the span length increases. On the first part of the Torino-Medicina link (red), the noise density is rather constant, indicating that the overall noise scales linearly with length, as expected in a homogeneous environment [35]. Interestingly, a lower noise density is observed in the urban Torino area. On the other hand, higher noise density is measured on segments including the metropolitan area of Milano, with its impact being progressively washed out when averaging over longer distances. The noise density of the Medicina-Firenze link (yellow) is considerably higher than on other spans, although the reason for that is unknown. On the

Firenze-Pozzuoli link (green), the noise density shows weak dependence on the length, which might be related to the absence of large metropolitan areas along the fiber path. On the Pozzuoli-Matera link (blue), the noise density is affected by the presence of aerial paths. Overall, these measurements confirm the large variability of noise levels recorded in land fibers, mostly due to the acoustic environment to which they are exposed. Although the noise levels recorded on this backbone are considerably higher as compared to other infrastructures realized elsewhere (see [38] for a comparison), efficient rejection can be achieved through Doppler noise cancellation up to acoustic frequencies, preserving the phase coherence between the launched and the received signal.

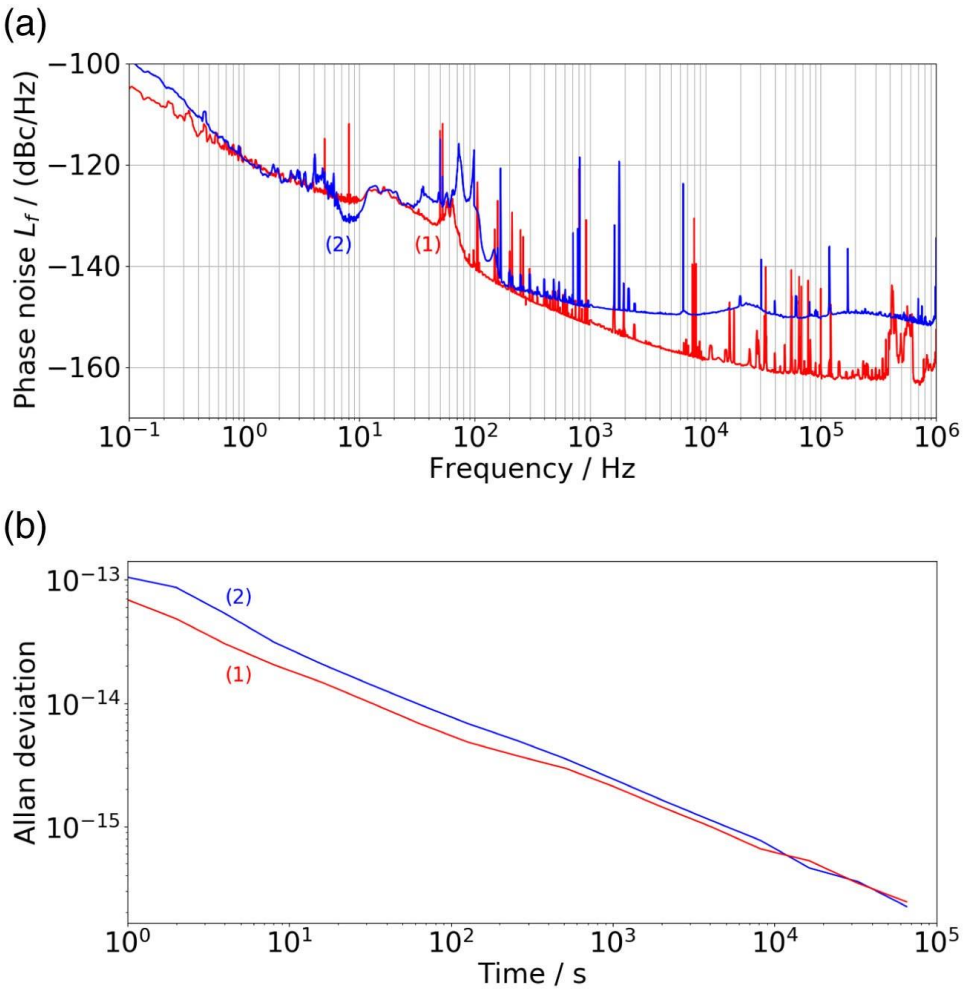

Figure 4: (a) Phase noise of the RF signal generated in Medicina (red, labeled 1) and Matera (blue, labeled 2) as compared to local hydrogen masers. Phase noise is referred to 10 MHz. (b) Allan deviation from three days of continuous comparison between the local masers and the link-disseminated RF signal in Medicina (red, labeled 1) and Matera (blue, labeled 2). The linear frequency drift of hydrogen masers was removed.

At each telescope, the comb-synthesized RF signal, which is referenced to the INRIM hydrogen maser, is constantly compared to the local maser. Figure 6.23(a) shows the phase noise of the comparisons in Medicina (red curve, 1) and Matera (blue curve, 2) at 10 MHz. The signature of the residual link noise is visible at acoustic frequencies between 1 and 100 Hz, while for lower frequencies, the measurement is limited by the noise floor of local hydrogen masers. The comparison in Matera shows a higher noise floor in the range 1 kHz to 1 MHz, which is consistent with the specified noise of the local hydrogen maser. Spurious signals at harmonics of the 50 Hz power line frequency are introduced by the RF dividers and the measurement chain. Figure 6.23(b) shows the long-term instability, in terms

of the Allan deviation, of a three-day pairwise frequency comparison after the linear drift of the hydrogen maser frequency is removed. The measured instabilities are in agreement with the local hydrogen masers' specifications, indicating no contribution from the dissemination chain. Unlike RF dissemination techniques, optical frequency dissemination allows the distribution of clock signals with higher stability than hydrogen masers and the effective implementation of a common-clock architecture.

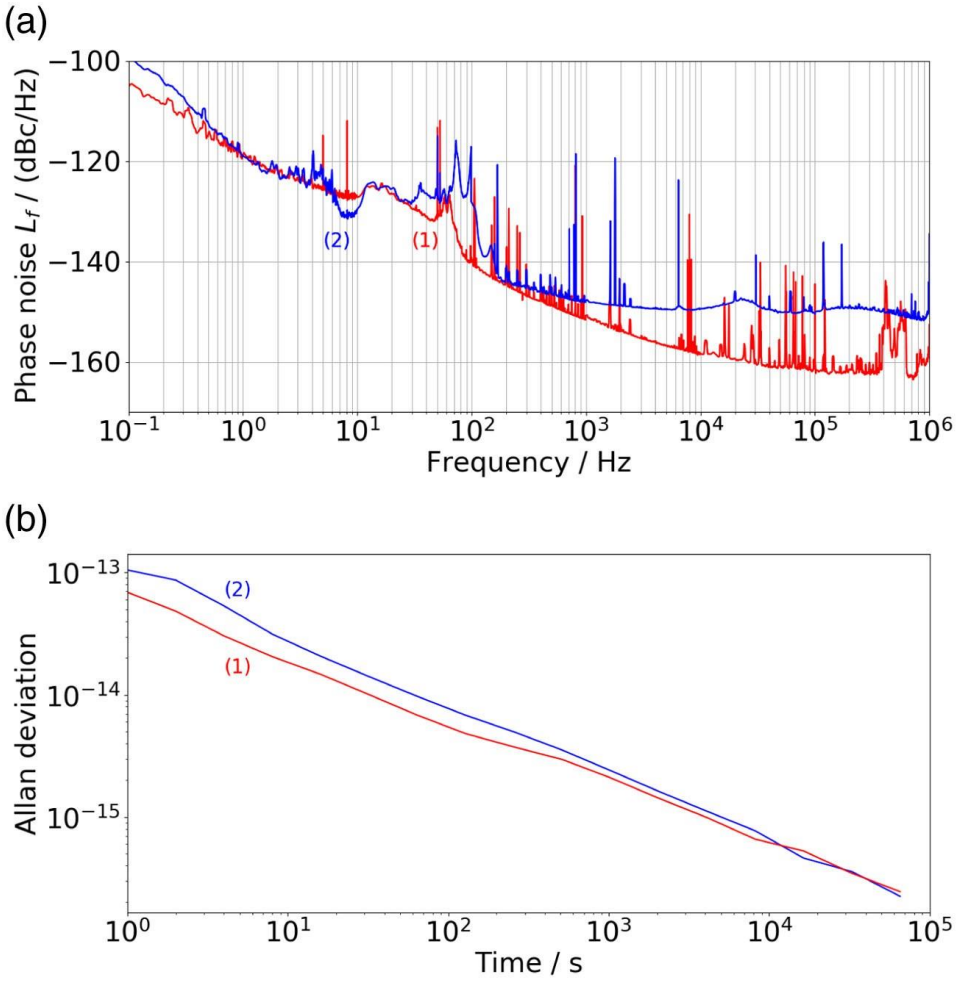

Figure 5: (a) Phase noise of the RF signal generated in Medicina (red, labeled 1) and Matera (blue, labeled 2) as compared to local hydrogen masers. Phase noise is referred to 10 MHz. (b) Allan deviation from three days of continuous comparison between the local masers and the link-disseminated RF signal in Medicina (red, labeled 1) and Matera (blue, labeled 2). The linear frequency drift of hydrogen masers was removed.

We note that the offline comparison described here is not strictly required in VLBI observations, where the fiber-delivered optical signal is scaled to the RF domain and directly employed in the synthesis chain instead of the local hydrogen maser. Nevertheless, it allows continuous calibration of local masers at a much higher resolution than currently available at VLBI sites, which is based on satellite techniques. This feature still offers the possibility of absolute referencing of VLBI frequency standards while relaxing reliability constraints in the dissemination chain, as offline calibration does not require continuous uptime owing to the high predictability of the hydrogen maser behavior. In addition, the combination of local and remote frequency standards could be an option in case of longer or noisier fiber segments, considering the limited bandwidth of the fiber noise cancellation. This approach combines the long-term stability and traceability to primary standards offered by fiber-based dissemination with the higher spectral purity of local oscillators in the 10 Hz to 1 kHz range.

During May 2019, we routinely compared the masers in Torino, Medicina, and Matera. The total measurement time, resulting from the combined uptime of all steps of the chain within the measurement campaigns, exceeded 200 h. Hydrogen masers were also compared in the same time intervals using geodetic Global Positioning System (GPS) receivers installed at the two telescopes. The difference between results of the hydrogen maser comparisons obtained using the fiber or the GPS is shown in Table 1 for the baselines Medicina-INRIM and Matera-INRIM,

Table 1.Results of the Closure Test between Fiber-Based and GPS Comparison of the Hydrogen Masers at INRIM, Medicina, and Matera

$(\text{Medicina} - \text{INRIM})_{\text{fiber}} - (\text{Medicina} - \text{INRIM})_{\text{GPS}} = (0.15 \pm 0.69) \times 10^{-15}$
$(\text{Matera} - \text{INRIM})_{\text{fiber}} - (\text{Matera} - \text{INRIM})_{\text{GPS}} = (-2 \pm 2) \times 10^{-15}$

and shows agreement within the limits set by the GPS resolution. In particular, a higher uncertainty is observed on the GPS baseline Torino-Matera due to higher instability of the GPS receiver in Matera.

The infrastructure was used in a geodetic VLBI campaign in which Medicina and Matera telescopes were operated in a common-clock architecture, using the frequency reference disseminated from INRIM as input for the VLBI synthesis chain. The campaign was a standard geodetic VLBI run lasting 24 h between May 19, 2019, 07:00UT and May 20, 2019, 07:00UT. The experiment described here consisted in several scans with varying duration of few minutes, during which a list of radio sources selected from the International Celestial Reference Frame version 2 (ICRF2)[39] was observed. The analysis was performed following the standard geodetic routine: the observation delays for each baseline are combined into a multiple parameter least squares fit, where effects such as Earth's orientation, station coordinates, ionospheric and tropospheric delays, and clocks' phase differences are taken into account. Each of these effects is modelled by specific relations and free parameters, whose best estimates are produced as output at the end of the least squares adjustment process. In preparation to this test, several campaigns with duration between 6 and 24 h were performed since 2017 involving Medicina and Matera radiotelescopes as well as other Italian and European stations. In such preliminary tests, Medicina, at the time the only station reached by the optical fibre, was operated using either the local or the fiber-disseminated signal, and no significant differences were observed in the quality of the results.

In the present experiment, the lock of the ultrastable laser to the hydrogen maser at INRIM was lost, as a consequence of permanent damage of the INRIM optical comb. This led to a highly nonlinear wander of the disseminated laser frequency, with short-term drifts as high as 5×10^{-15} /s, and instantaneous deviations from the nominal frequency value of up to 2×10^{-12}. These performances are several orders of magnitude worse than that of a hydrogen maser, whose typical frequency drift is $<10^{-15}$/day. We chose to perform the common-clock VLBI campaign even in such a challenging condition, given the limited availability of observing time at the antennas and the difficulty in rescheduling the experiment. In fact, the clocks' frequency deviations are expected to be highly correlated in Matera and Medicina, as the same signal is distributed to both sites. The analysis of the experiment verified this hypothesis, by retrieving this information from VLBIdata.

A least-squares fit to the group delays is performed on the scans of the Medicina-Matera baseline over 15 h of data free from clock breaks; 181 out of 238 scans (76%) were used in the analysis because of RF interference and anomalous noise in the receivers, which did not depend on the fiber-disseminated frequency reference. Fit residuals are shown in Figure 6.24 for valid scans. The weighted root mean

square value of residuals is 58ps.Typicalvalues of residuals on standard geodetic campaigns involving Medicina or Matera telescopes on international baselines range between 15 ps and 60 ps, where the variability depends on several factors, including the number of telescopes and baselines, experimental conditions, and data quality. The value obtained in this experiment allowed standard geodetic analysis and confirms the suitability of common, fiber-disseminated clock signals to VLBI observations.

For the considered period, the time delay *1t* between the clocks in Medicina and Matera was modelled in the least squares adjustment process as

$$\Delta t = t_0 + y_0(t - t_{start}) + d(t - t_{start})_2, \qquad (1)$$

where t_{start} is the start time of the considered period and t_0, y_0, and d are estimated by the algorithm. From Eq. (1) the instantaneous relative frequency difference between the two clocks is derived,

$$y = y_0 + 2d(t - t_{start}). \qquad (2)$$

The best fit estimation of the clocks' parameters during the considered experiment, derived from standard analysis, is $y_0 = (-0.43 \pm 1.16) \times 10^{-14}$ and $d = (-1.46 \pm 1.66) \times 10^{-14}$/day. The result shows that within the uncertainty set by the global solution, no difference is appreciated between the two clock signals delivered at each of the VLBI facilities. This result is in agreement with the assumption that the telescopes in Medicina and Matera actually shared the same clock, and confirms that the realized infrastructure does not introduce additional noise to the system and can be effectively exploited in VLBI campaigns. We note that such results were obtained in exceptional experimental conditions where the frequency instability of the disseminated signal was much worse than that of a typical H-maser. Still, this did not lead to major anomalies in the experimental outcome owing to the fact that the same frequency signal was delivered to both telescopes. Higher-order effects might have been present, which, however, are not observed within the current measurement uncertainty.

Building on this experiment, future campaigns are planned. On one hand, collecting more statistics will allow the quantitative assessment of improvements achievable by operating the telescopes in a common-clock topology. On the other hand, we will investigate how this topology could be exploited to reduce the problem complexity from the statistical point of view.

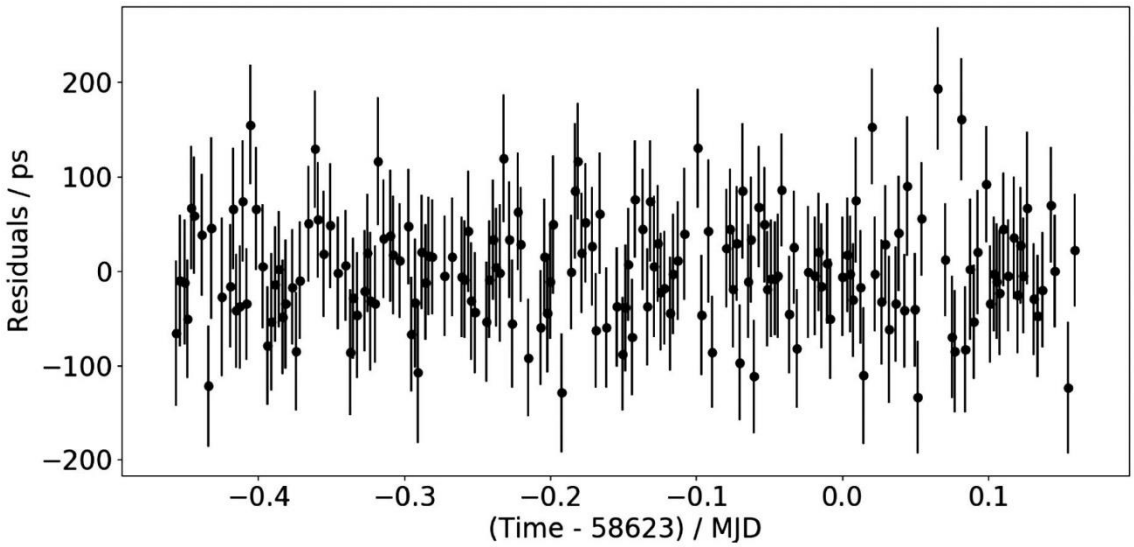

Figure 6: Residuals on the group delay versus observing time as a result of the geodetic analysis of the May, 19–20, 2019, observing session on the baseline Medicina-Matera. Every data point represents a single scan.

2.5 Antimatter spectroscopy and the search for new physics

The existence of antimatter is a consequence of the Charge-Parity-Time symmetry of the standard model of fundamental physics. Studies of antimatter can provide stringent tests of this symmetry and therefore of the standard model, with the potential for discovering new physics, i.e. phenomena which are not included in or contradict the theory of the fundamental nature of the universe. Thus, for example, CERN has a programme dedicated to antimatter studies [41], which includes several experiments. One of these is ASACUSA [42], one aspect of which is spectroscopy involving antimatter, in particular antihydrogen, in order to compare with previous extremely precise spectroscopic measurements of hydrogen. In the medium-long term such experiments will require very high accuracy frequency references, and the means to compare them with references on other sites. Beyond these specific CERN projects, there are many ways in which high-precision spectroscopy experiments, especially carried out over distributed networks, may contribute to the discovery of new physics, as explained for example in the science case deliverable of CLONETS-DS [43]. The relevant research community in Europe is actively developing proposals for such science, for example in the context of the Quantum and Emerging Technologies Detectors axis of the European Committee for Future Accelerators roadmap [44]. The proposed fibre infrastructure for time and frequency dissemination in the European Research Area will play a central role in such work.

2.6 Telecommunications

Internet and mobile communications are changing the world and telecom networks are one of the underlying infrastructures facilitating this change. New 5G networks will have a substantial impact on society through the internet of things, smart cities, smart transportation and explosion of e-Commerce. Stringent time synchronisation (better than a few microseconds) is already required for the generation of signals over the air interface of mobile systems supporting synchronous interworking. Phase synchronisation is required in Multimedia Broadcast/Multicast Service (MBMS) when it is based on single-frequency network (MBSFN) mode, motivated by the densification of the network. In this latter case the timing must be much more accurate than the actual capability of the WCDMA node synchronisation function. These requirements are incorporated in the Recommendation ITU-T G.8271/Y.1366, which also includes the so called “hybrid” network, based on the coexistence of a synchronous and an asynchronous layer. Telecommunication companies have already foreseen a requirement for a timing instability better than 20 ns at all core-locations, better than 1 ns between core locations, and one UTC reference location which should be connected to a UTC(k) reference with a timing instability significantly better than 100 ps, which is not possible for current T/F dissemination facilities that are not based on fibre optic.

In this case, dissemination of time over fibre can offer those levels of synchronization both using technique like PTP High Accuracy (also known as White Rabbit), and Electronic Stabilised techniques (ELSTAB [45]).

3 Conclusions

This document has illustrated the impact of the pan-European fibre infrastructure for time and frequency dissemination proposed by CLONETS-DS on research in the European Research Area, by providing details of how the infrastructure will be used for key applications, and thus aims to facilitate the uptake of the infrastructure for those applications. It also summarised the fibre infrastructures for time and frequency dissemination which are currently being operated by the CLONETS-DS partners, and the possibilities for using them for proof-of-concept demonstrations.

Glossary

ACONet	Austrian Academic Computer Network
AIPS	Astronomical Image Processing System
ALMA	Atacama Large Millimetre Array
CITAF	Czech Infrastructure for Time and Frequency
CLONETS	Clock Network Services
CLONETS-DS	Clock Network Services Design Study
CTR	Compact Triple-band Receiver
CSO	Cryogenic Sapphire Oscillator
ECN	European Core Network
EOP	Earth Orientation Parameters
FFR	Fractional Flux Recovery
FPT	Frequency Phase Transfer
KVN	Korean VLBI Network
LUH	Leibniz Universität Hannover
MJD	Modified Julian Day or Date
MPQ	Max Planck Institute of Quantum Optics
NMI	National Metrology Institute
PTB	Physikalisch- Technische Bundesanstalt
REFIMEVE	REseau Fibré MEtrologique à Vocation Européenne
RMS	Root Mean Square
SNR	Signal-to-Noise Ratio
UT	Universal Time
UT1	A realization of UT
UTC	Coordinated Universal Time
UTC(k)	A realisation of UTC by the entity identified by “k”
VGOS	VLBI Global Observing System
VLBI	Very Long Baseline Interferometry

References

[1] "Deliverable D2.1 Technical Design Report", CLONETS-DS project, https://clonets-ds.eu.

[2] Rioja M. & Dodson R. 2020, "Precise radio astrometry and new developments for the next-generation of instruments", A&ARv, vol 28, pg. 6.

[3] Rioja M. et al., 2012, "The Impact of Frequency Standards on Coherence in VLBI at the Highest Frequencies", Astronomical Journal, vol 144, pg. 121.

[4] Rioja, M., & Dodson, R. 2011 "High-precision Astrometric Millimeter Very Long Baseline Interferometry Using a New Method for Atmospheric Calibration", AJ, 141, 114.

[5] Lee, S.-S., et al., 2014, "Early science with the Korean VLBI network: Evaluation of system performance", AJ, vol 147, pg. 77.

[6] Han S.T., et al., 2013, "Korean VLBI Network Receiver Optics for Simultaneous Multifrequency Observation: Evaluation", PASP, vol. 125, pg. 539.

[7] Rioja, M., et al. 2015, "The Power of Simultaneous Multifrequency Observations for mm-VLBI: Astrometry up to 130 GHz with the KVN", Astronomical Journal, Volume 150, Issue 6, article id. 202, 14pp.

[8] Sovers O.J., Fanselow J.L., & Jacobs C.S., 1998, "Astrometry and geodesy with radio interferometry: experiments, models, results" Rev. Mod. Phys. 70, 1393.

[9] Schuh, H. & Behrend D., 2012, "VLBI: A fascinating technique for geodesy and astrometry", Journal of Geodynamics, Vol 61, pg. 68-80.

[10] Petrachenko, B., Niell, A., Behrend, D., Corey, B., Bohm, J., Charlot, P., et al. (2009). "Design aspects of the VLBI2010 system. Progress report of the VLBI2010 committee" (Tech. Rep.): NASA/ TM-2009-214180, NASA Technical Memorandum. https://ivscc.gsfc.nasa. nasa.gov/publications/misc/ TM-2009-214180.pdf

[11] Niell, A., Barrett, J., Burns, A., Cappallo, R., Corey, B., Derome, M., et al. (2018). "Demonstration of a broadband very long baseline interferometer system: A new instrument for high-precision space geodesy". Radio Science, 53, 1269–1291. https://doi.org/10.1029/2018RS006617

[12] Deller, A.T., et al. 2007, "DiFX: A Software Correlator for Very Long Baseline Interferometry Using Multiprocessor Computing Environments", PASP, vol. 119, pg. 318.

[13] Sekido M., et al. 2021, "A broadband VLBI system using transportable stations for geodesy and metrology: an alternative approach to the VGOS concept", Journal of geodesy, Vol. 95, Article number 41.

[14] M. Pizzocaro et al., « Intercontinental comparison of optical atomic clocks through very long baseline interferometry », Nature Physics, vol. 17, no 2, Art. no 2, févr. 2021, doi: 10.1038/s41567-020-01038-6.

[15] Clivati C. et al. 2020, "Common-clock very long baseline interferometry using a coherent optical fiber link", Optica, vol. 7, issue 8, pg. 1031.

[16] Mehlstäubler T.E., et al 2018, "Atomic clocks for geodesy", Rep. Prog. Phys. 81 064401.

[17] Bjerhammar, A., 1975. “Discrete approaches to the solution of the boundary value problem in physical geodesy”. Boll. di Geodesia e Scienze Affini, 185-240.

[18] Bjerhammar, A., 1985. “On a relativistic geodesy”. Bull. Géod. 59, 207–220.

[19] Vermeer M. 1983 Chronometric levelling Reports of the Finnish Geodetic Institute, 83 1-7.

[20] Hooijberg M., 2008, “Geometrical Geodesy”, Springer Editions.

[21] Denker H., 2013, in *Sciences of Geodesy – II: Innovations and Future Developments* (ed. Xu, G.) Ch. 5, Springer Editions.

[22] Bondarescu, R., Schärer, A., Lundgren, A., Hetényi, G., Houlié, N., Jetzer, P., Bondarescu, M., 2015. Ground- based optical atomic clocks as a tool to monitor vertical surface motion. Geophys. J. Int. 202, 1770–1774. doi:10.1093/gji/ggv246.

[23] Wilkinson M. Et al., “The next generation of satellite laser ranging systems ” Journal of Geodesy (2019) 93:2227–2247.

[24] Altamimi Z., et al. 2016, “ITRF2014: A new release of the International Terrestrial Reference Frame modeling nonlinear station motions” JGR Solid Earth, Vol. 121, issue 8, pg. 6109-6131.

[25] Pearlman M, Noll C, McGarry J, Gurtner W, Pavlis E (2009) “The international laser ranging service”. Adv Geosci 13:129–153.

[26] Exetier P. Et al., 2017, “Time biases in laser ranging observations: A concerning issue of Space Geodesy”, Advances in Space Research, vol 60, pg. 948-968.

[27] Exetier P. Et al., 2019, “Time and laser ranging: a window of opportunity for geodesy, navigation, and metrology”, Journal of Geodesy, vol 93, pg. 2389-2404.

[28] Meng W, Zhang H, Huang P et al (2013) “Design and experiment of onboard laser time transfer in Chinese Beidou navigation satellites”. Advances in Space Research vol 51: pg. 951–958.

[29] Samain E et al (2008) “T2L2 experiment on Jason-2 and further experiments”. Int J Mod Phys D 17(7):1043–1054.

[30] Hess MP, Stringhetti L, Hummelsberger B, Hausner K, Stalford R, Nasca R, Léger B et al (2011) “The ACES mission: system development and test status”. Acta Astronautica 69(11-12):929–938.

[31] Nanni, M. Negusini, F. Perini, M. Roma, M. Stagni, M. Zucco, and D. Calonico, “A VLBI experiment using a remote atomic clock via a coherent fiber link,” Sci. Rep. 7, 40992 (2017).

[32] L. F. Livi, G. Cappellini, M. Diem, L. Franchi, C. Clivati, M. Frittelli, F. Levi, D. Calonico, J. Catani, M. Inguscio, and L. Fallani, “Synthetic dimensions and spin-orbit coupling with an optical clock transition,” Phys. Rev. Lett. 117, 220401 (2016).

[33] G. Insero, S. Borri, D. Calonico, P. C. Pastor, C. Clivati, D. D’Ambrosio, P. De Natale, M. Inguscio, F. Levi, and G. Santambrogio, “Measuring molecular frequencies in the 1–10 micron range at 11-digits accuracy,” Sci. Rep. 7, 12780 (2017).

[34] M. Pizzocaro, F. Bregolin, P. Barbieri, B. Rauf, F. Levi, and D. Calonico, “Absolute frequency measurement of the transition of with a link to international atomic time,” Metrologia 57, 035007 (2020).

[35] P. A. M. Williams, W. C. Swann, and N. R. Newbury, “High-stability transfer of an optical frequency over long fiber-optic links,” J. Opt. Soc. Am. B 25, 1284–1293 (2008).

[36] F. Guillou-Camargo, V. Ménoret, E. Cantin, O. Lopez, N. Quintin, E. Camisard, V. Salmon, J.-M. Le Merdy, G. Santarelli, A. Amy-Klein, P.-E. Pottie, B. Desruelle, and C. Chardonnet, "First industrial-grade coherent fiber link for optical frequency standard dissemination," Appl. Opt. 57, 7203–7210 (2018).

[37] C. Clivati, P. Savio, S. Abrate, V. Curri, R. Gaudino, M. Pizzocaro, and D. Calonico, "Robust optical frequency dissemination with a dual-polarization coherent receiver," Opt. Express 28, 8494–8511 (2020).

[38] C. Clivati, A. Tampellini, A. Mura, F. Levi, G. Marra, P. Galea, A. Xuereb, and D. Calonico, "Optical frequency transfer over submarine fiber links," Optica 5, 893–901 (2018).

[39] A. L. Fey, D. Gordon, C. S. Jacobs, C. Ma, R. A. Gaume, E. F. Arias, G. Bianco, D. A. Boboltz, S. Bockmann, and S. Bolotin, "The second realization of the International Celestial Reference Frame by very long baseline interferometry," Astron. J. 150, 58 (2015).

[40] M. B. K. Tønnes, "Understanding and exploiting metrological fiber networks for Sagnac sensing, frequency dissemination and geosensing", PhD thesis, (2022), https://theses.hal.science/tel-03984045v1

[41] CERN site devoted to antimatter, https://home.cern/science/physics/antimatter

[42] ASACUSA Atomic Spectroscopy And Collisions Using Slow Antiprotons, https://asacusa.web.cern.ch/

[43] **"**Deliverable D1.2 Requirements and Definitions", CLONETS-DS project, https://clonets-ds.eu

[44] European committee for Future Accelerators, https://ecfa.web.cern.ch/

[45] P. Krehlik, Ł. Śliwczyński, Ł. Buczek, J. Kołodziej, and M. Lipiński, 'ELSTAB—Fiber-Optic Time and Frequency Distribution Technology: A General Characterization and Fundamental Limits', IEEE Transactions on Ultrasonics, Ferroelectrics, and Frequency Control, vol. 63, no. 7, pp. 993–1004, Jul. 2016, doi: 10.1109/TUFFC.2015.2502547.